

Visibility graph analysis of solar wind velocity

Vinita Suyal¹ · Awadhesh Prasad² ·
Harinder P. Singh³

© Springer ●●●

Abstract We analyze *in situ* measurements of solar wind velocity obtained by Advanced Composition Explorer (ACE) spacecraft and Helios spacecraft during the years 1998 – 2012 and 1975 – 1983 respectively. The data belong to mainly solar cycle 23 (1996 – 2008) and solar cycle 21 (1976 – 1986) respectively. We use Directed Horizontal Visibility graph (DHVg) algorithm and estimate a graph functional, namely, the degree distance (D) as the Kullback-Leibler divergence (KLD) argument to understand time irreversibility of solar wind time series. We estimate this degree distance irreversibility parameter for these time series at different phases of solar activity cycle. Irreversibility parameter is first established for known dynamical data and then applied for solar wind velocity time series. It is observed that irreversibility in solar wind velocity fluctuations show similar behavior at 0.3 AU (Helios data) and 1 AU (ACE data). Moreover it changes over the different phases of solar activity cycle.

Keywords: Solar wind velocity; Solar activity cycle; Horizontal visibility graph; irreversibility

1. Introduction

Solar wind is the continuation of the solar corona and it continuously expands into space with speeds that can vary from about 250 km/s to more than 800 km/s (Schwenn, 2007). The interaction between solar wind and the local interstellar medium determines the size and boundaries of the heliosphere (Balogh, Suess, and Lanzerotti, 2008). Solar wind is a turbulent plasma and this turbulence is anisotropic with respect to the mean magnetic field (Robinson and Rusbridge, 1971; Shebalin, Matthaeus and Montgomery, 1983; Goldreich and Sridhar, 1995). Solar wind variability (velocity, proton density, temperature, and helium content) leads to evolving, dynamic phenomena throughout the heliosphere on all temporal and spatial scales (Goldstein, Roberts and Matthaeus, 1995). Solar wind velocity shows a high correlation with coronal holes area (Rotter *et al.*, 2012).

^{1,2,3}Department of Physics and Astrophysics, University of Delhi, Delhi 110007, India.

email:¹vinita.suyal@gmail.com

²awadhesh@physics.du.ac.in

³hpsingh@physics.du.ac.in

These coronal holes are long-lived structures on the Sun, which may persist for several solar rotations.

Solar wind has a three-dimensional structure and it is highly dependent upon solar cycle (Hapgood *et al.*, 1991; McComas *et al.*, 2003; Schwenn, 2007; Balogh, Suess, and Lanzerotti, 2008). Its characteristics vary over a solar cycle, but it maintains its simplest configuration during solar activity minimum, when large polar coronal holes dominate the outer solar atmosphere away from the equator (Hansteen and Velli, 2012). Due to overlapping of fast streams from the coronal holes at the solar maximum, solar wind velocity time series has larger fluctuations (Katsavrias, Preka-Papadema, and Moussas, 2012; Suyal, Prasad, and Singh, 2012a).

The analysis of solar wind plasma has been an area of considerable research interest in recent past. Various complexity measures such as entropy (Macek and Obojska, 1997, 1998; Macek and Redaelli, 2000; Redaelli and Macek, 2001; Suyal, Prasad, and Singh, 2012a), Lyapunov exponents (Macek and Obojska, 1998; Redaelli and Macek, 2001; Gupta *et al.*, 2008) and correlation dimension (Macek and Obojska, 1997; Gupta *et al.*, 2008) show that solar wind velocity fluctuations are a consequence of complex nonlinear dynamical processes. Milano *et al.*, 2004 suggested an anisotropy in the velocity, magnetic, and cross helicity correlation function and power spectra by analyzing magnetic and bulk velocities measured by ACE. Gupta *et al.*, 2008 analyzed the solar wind velocity data to observe the inherent changes in the dynamics governing the solar wind at 0.3 AU. Suyal, Prasad, and Singh, 2012b analyzed the correlation of solar wind velocity at different phases of the solar activity cycle. They suggested hysteresis in the dynamics governing the solar wind over a complete solar activity cycle (Suyal, Prasad, and Singh, 2012a).

In the present work, we analyze the solar wind velocity time series at different phases of solar activity cycle. We use the data obtained from ACE during 1998 – 2012 and Helios spacecraft during 1975 – 1983. ACE data belong mainly to the solar activity cycle 23, while data obtained from Helios spacecraft correspond to solar activity cycles 21. We estimate the time irreversibility parameter, D using directed horizontal visibility graph (DHVg) algorithm (Lacasa *et al.*, 2012) for the solar wind time series. In the next section, we review the DHVg algorithm to calculate D of time series. In Section 3 we estimate D for known dynamical systems. In Section 4, we analyze solar wind data using DHVg technique. It is followed by conclusions in Section 5.

2. Directed horizontal visibility graph algorithm

Let $x_i, i = 1, 2, \dots, N$, be a time series such that $x_{i+1} = x_i + \delta t$, where δt is the sampling time. Fig. 1 shows a time series of 6 data points. As per DHVg algorithm (Lacasa *et al.*, 2012), each data point is treated as a node of a graph. Two nodes i and j are said to be connected if

$$x_i, x_j > x_n \forall n; i < n < j. \quad (1)$$

For example, in Fig. 1, nodes 1 and 3 are connected whereas nodes 1 and 5 are not connected. Now an ingoing degree for i^{th} node, $k_{in}(i)$ is defined as the number

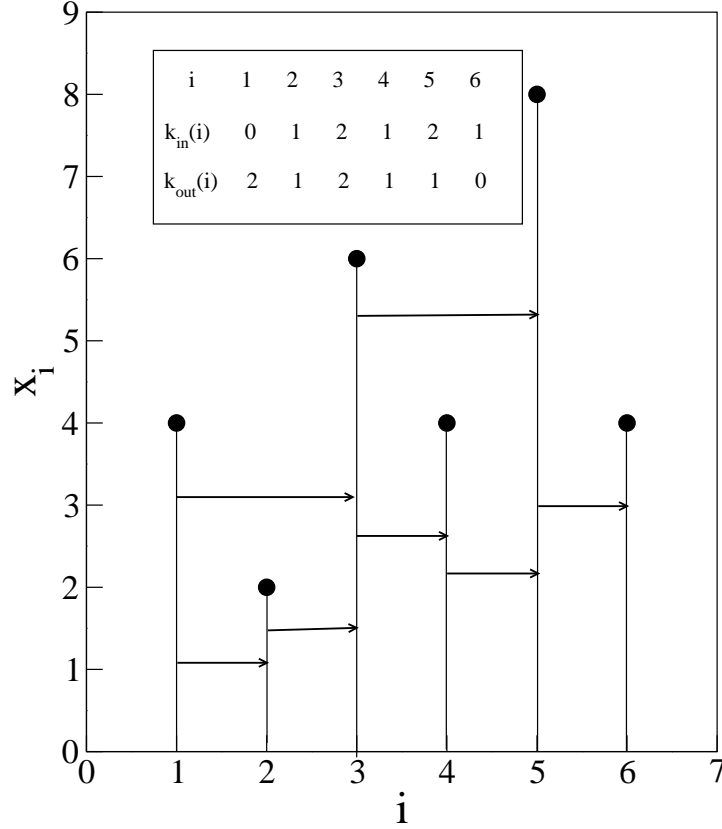


Figure 1. Graphical representation of a time series of 6 data points. Arrows show the ‘visibility’. Ingoing degree $k_{in}(i)$ and outgoing degree $k_{out}(i)$ are mentioned in the inset.

of links of that node with other past nodes. Similarly an outgoing degree $k_{out}(i)$ is defined as the number of links with future nodes. Corresponding to each node of time series shown in the Fig. 1, k_{in} and k_{out} are written in the inset. Now degree $k(i)$ of i^{th} node can be written as

$$k(i) = k_{in}(i) + k_{out}(i). \quad (2)$$

The degree distribution of a graph gives the probability of an arbitrary node to have degree k (Newman, 2003). Let $P_{in}(i)$ and $P_{out}(i)$ denote the probability distributions of ‘in’ and ‘out’ degree distributions respectively.

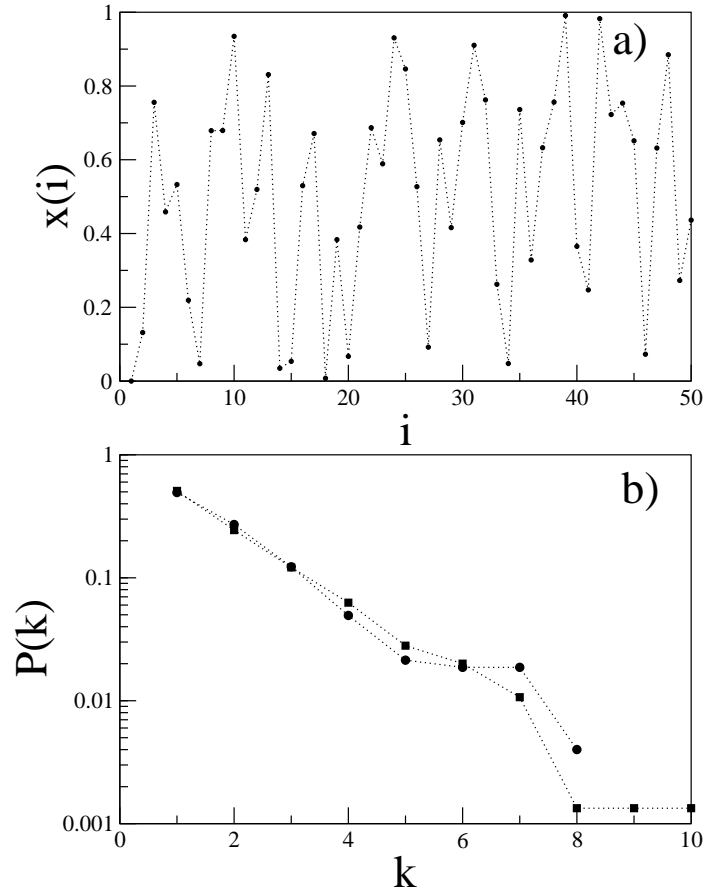


Figure 2. (a) Random numbers (50 points) uniformly distributed in the range $[0 - 1]$. (b) *In* (●) and *out* (■) degree distributions for the time series shown in (a) (for 750 data points).

Lacasa *et al.*, 2012 suggested that Kullback-Leibler divergence (KLD) (Cover and Thomas, 2006) between the *in* and *out* degree distributions,

$$D(P_{out} \parallel P_{in}) = \sum_i P_{out}(i) \log \frac{P_{out}(i)}{P_{in}(i)}, \quad (3)$$

can be used as a measure of the irreversibility of two real-valued stochastic series. D vanishes if both the probability distributions are equal. The more distinguishable are P_{out} and P_{in} with respect each to other, the larger is the parameter D and hence more time irreversible the series is.

3. Irreversibility of a time series

In order to understand the time irreversibility in a system using DHVg, we take few examples. In all the examples we take time series of length 750 data points as the shortest solar wind time series available is consists of approximately 750 points. First we generate a time series of uniformly distributed random numbers in the range $[0, 1]$. Fig. 2 (a) shows first 50 points of this time series. In Fig. 2 (b) we show the *in* and *out* degree distributions of DHVg for this time series of 750 data points. We estimate D for this data and find it to be very close to zero. For second example, we take Arnold cat map (Arnold and Avez, 1968),

$$\begin{aligned}x_{t+1} &= x_t + y_t \text{ mod}(1), \\y_{t+1} &= x_t + 2y_t \text{ mod}(1).\end{aligned}\tag{4}$$

This is an example of a conservative chaotic system, and the time series obtained from this map is reversible in time. We estimate the irreversibility parameter D for this time series and observed that it is also very close to zero (Lacasa *et al.*, 2012). Now we consider the case of a dissipative and hence time irreversible system, for example logistic map in the chaotic regime,

$$x_{t+1} = 4x_t(1 - x_t).\tag{5}$$

The estimated value of D for the time series corresponding to logistic map is significantly larger than that the reversible ones. We plot D for all these time series, i.e. obtained from area preserving (e.g., random time series and Arnold cat map) and dissipative (e.g., logistic map) systems in Fig. 3. This figure clearly distinguishes the reversibility in these different type of systems. These deterministic models are used just to demonstrate the usefulness of the DHVg analysis.

In order to see the effect of length of the time series on the irreversibility parameter we estimate D for different lengths. Fig. 4 shows the plot of $D[P_{out} || P_{in}]$ vs. lengths of the time series obtained from different systems as considered above. This plot shows that for a uniform random distributed time series (●) and time series generated from Arnold cat map (▲), the value of D are small which tends to zero as the length of the time series increases. However for irreversible system (logistic map, ■) value of D remains significantly large as compared to that for the reversible system (uniformly distributed random data or generated from Arnold map) for different length of time series. This suggests that 750 data points are thus sufficient to use DHVg measures to understand the irreversibility in time series. Therefore we consider this number of data points to find the D for solar wind data as discussed below.

4. Visibility graph analysis of solar wind data

The Advanced Composition Explorer was launched on August, 1997 to measure the elemental, isotopic, and ionic charge-state composition of nuclei from solar wind energies ($\sim 1\text{KeV nucl}^{-1}$) to galactic cosmic-ray energies ($\sim 500\text{MeV}$

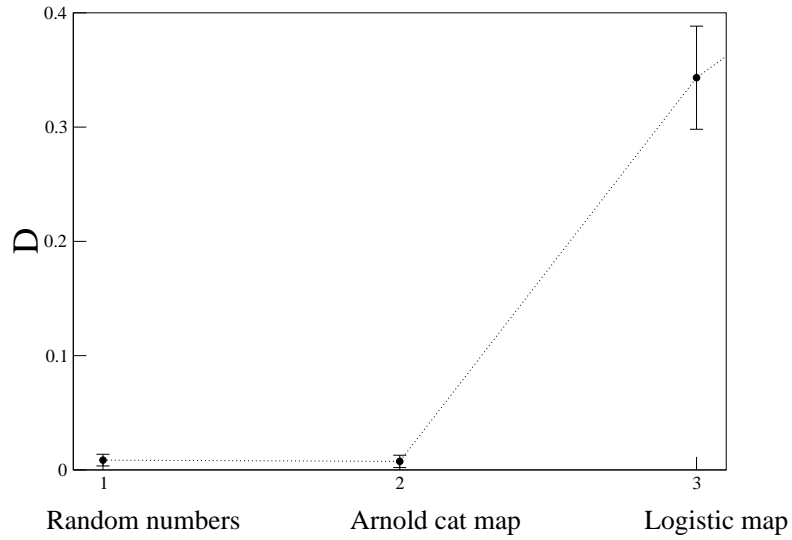


Figure 3. Distance, D , for area preserving (e.g., uniformly distributed random numbers and Arnold cat map) and dissipative (e.g., logistic map) with 750 data points each. 1σ error bars are shown where σ is the standard deviation.

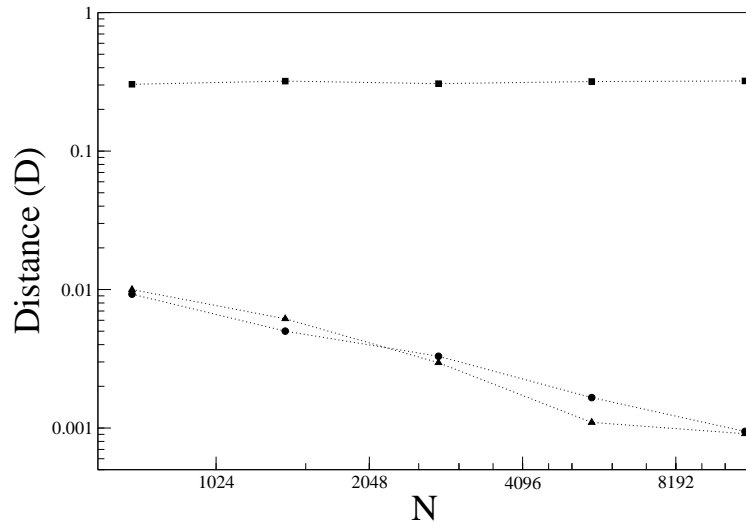


Figure 4. Plot of $D[P_{out} || P_{in}]$ of the graph associated to random number data (●), data obtained from logistic map in the chaotic regime (■), and Arnold cat map (▲) as a function of the series of length N .

nucl^{-1}) (Stone *et al.*, 1998). These data cover most of the solar activity cycle 23 and a part of solar cycle 24. We use hourly averaged solar wind velocity data at a distance of 1 AU obtained from the Solar Wind Ion Composition Spectrometer (SWICS) on ACE (<http://www.srl.caltech.edu/ACE/ASC/level2/>). Due to data gap in the archive, we split the data set into 22 continuous small time series. The details of the time series used are given in Table 1. Fig. 5 (a) shows a typical time series of solar wind velocity obtained from ACE spacecraft during 1998. In Fig. 6 (a) we plot smoothed monthly averaged sunspot number (<http://sidc.oma.be/sunspot-data/>) during the same period. Serial numbers show the corresponding solar wind data sets on the smoothed sunspot index curve.

Table 1. Initial time (T), of the 22 time series of hourly averaged solar wind velocity data measured by the ACE spacecraft from 1998 to 2012. Third column gives time irreversibility parameter, D (Eqn. 3). The last column gives the smoothed monthly averaged sunspot numbers (SSN).

S.No.	T	N	D	SSN
1	1998.25	1665	0.0595	55.0
2	1998.71	1314	0.0785	69.5
3	1998.91	789	0.0391	75.0
4	1999.11	1927	0.0152	84.6
5	1999.41	2716	0.0446	91.6
6	1999.73	1139	0.0314	102.3
7	1999.94	1404	0.0391	111.1
8	2000.15	3075	0.0477	116.8
9	2000.88	1580	0.0402	112.7
10	2001.40	1315	0.0324	109.4
11	2002.03	3329	0.0619	113.5
12	2002.41	3417	0.0332	107.5
13	2003.03	789	0.0182	80.8
14	2003.24	1840	0.0206	72.0
15	2003.90	2633	0.0313	55.7
16	2005.33	2541	0.0700	31.6
17	2006.45	2278	0.0761	16.3
18	2008.39	2108	0.0740	3.5
19	2010.18	1954	0.0443	12.3
20	2010.42	915	0.0504	15.9
21	2010.95	1182	0.0138	28.8
22	2011.89	867	0.0783	61.1

We follow four phases of a solar activity cycle namely, low activity region, ascending phase, high activity region, and descending phase. These phases/regimes are

Table 2. Initial time (T), of the 15 time series of 64 sec averaged solar wind velocity data measured by the ACE spacecraft from 1998 to 2012. Third column gives time irreversibility parameter, D (Eqn. 3). The last column gives the smoothed monthly averaged sunspot numbers (SSN).

S.No.	T	D	SSN
1	1998.20	0.0029	53.5
2	1999.16	0.0017	84.6
3	2000.04	0.0019	112.9
4	2001.16	0.0026	104.8
5	2002.75	0.0017	94.6
6	2003.01	0.0023	80.8
7	2004.01	0.0030	52.0
8	2005.02	0.0031	34.6
9	2006.05	0.0032	20.8
10	2007.05	0.0032	11.9
11	2008.01	0.0029	4.2
12	2009.01	0.0025	1.8
13	2010.04	0.0038	9.3
14	2011.15	0.0031	33.4
15	2012.02	0.0028	65.5

marked with alphabets, A , B , C and E respectively in Figs. 6, 7, and 9. Hourly averaged solar wind velocity data obtained from ACE is such that time series 1 and 2 belong to region B (ascending phase), time series 3 to 15 belong to region C (high activity region), and time series 15 to 18 belong to region E (the descending phase) of solar activity cycle 23. After time series 18, a new activity cycle 24 starts. Time series having serial numbers 21 and 22 resemble time series 1 and 2 of the previous activity cycle respectively.

We estimate D using DHVg analysis for all these 22 time series. Since all the series are of different lengths, we took 5 overlapping windows of 750 data points, estimate D for each window and then estimate the average value of the D . Fig. 6 (b) shows variation of D for solar wind velocity data corresponding to the years 1998 to 2012. We observe that estimated values of the irreversibility parameter D for time series corresponding to region B, *i.e.*, ascending phase of the activity cycle are larger than D for region C, *i.e.*, high activity region. D fluctuates in a narrow range for solar wind velocity data corresponding to this region. (except time series 11). As the activity decreases (region E), estimated values of D increase sharply. They reach a peak (for time series 17 and 18) at minimum activity. On the onset of new activity cycle, D decreases and similar behavior is observed in the ascending phase of the next solar activity cycle although the magnitude is different.

We also use 64 sec averaged solar wind velocity data during the same time period, *i.e.*, from 1998 to 2012. Table 2 gives the details of the time series used. Fig. 7 (a) shows the smoothed monthly averaged sunspot data and Fig. 7 (b) shows the variation of D during the different phases of the solar activity cycle

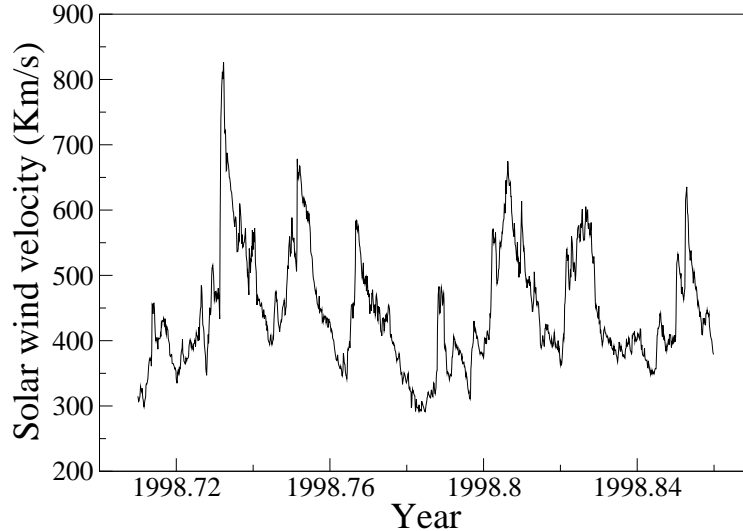


Figure 5. Time series of solar wind velocity data obtained from ACE spacecraft correspond to data set corresponds to S. No. 2 of Table 1.

for 64 sec averaged data. A comparison of Fig. 6 (b) and Fig. 7 (b) shows that the variation of D shows similar behavior for 64 sec and hourly averaged data.

Since we do not have ACE data for high activity region and descending phase of activity cycle 24, we consider another set of solar wind data which is obtained from Helios space probes. Helios space probes gathered solar wind data during part of solar cycle 20 and 21 i.e., between 1975 and 1983. They covered the heliocentric-distance from 0.28 AU to 1.0 AU. We analyze radial velocity measured by the Helios spacecraft at 0.3 AU corresponding to the part of the solar activity cycle 20 and 21. This data is obtained from http://sprg.ssl.berkeley.edu/impact/data_browser_helios.html. The details of the time series used are given in Table 3. Sampling time for each time series is 40.5 sec. In Fig. 8 (a), we have shown a representative solar wind time series obtained from Helios spacecraft. The time series shows a decreasing trend. Therefore, linear and quadratic trends were subtracted from the raw data (Macek and Obojska, 1997; Gupta *et al.*, 2008). Fig. 8 (b), shows the resulting detrended time series for the data. In Fig. 9 (a) we plot smoothed monthly averaged sunspot number with time during the years 1975 – 1983. The position of serial numbers corresponding to the solar wind data sets is shown. We denote region A (time series from 1-7), region B (time series from 8-12), C (time series from 13-17), and E (time series 17 and 18 on the activity cycle. In Fig. 9 (b), we plot D for all the 18 time series listed in Table 3. Fig. 9 shows that the number of sunspots does not change much for region corresponding to time series 1 to 9, and D fluctuates in narrow

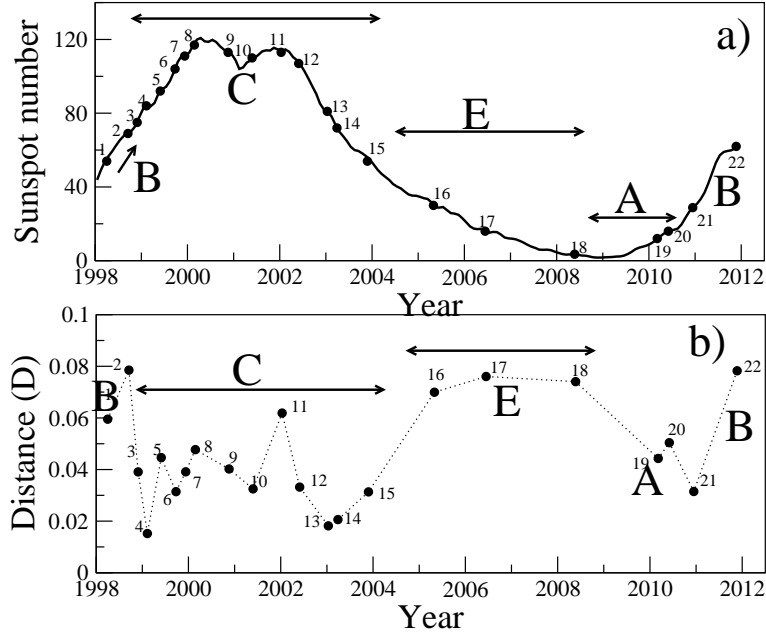


Figure 6. (a) Smoothed monthly averaged sunspot number from 1996 to 2012. Serial numbers 1 – 22 correspond to the solar wind data sets given in Table 1. Arrows with symbols A, B, C, and E indicate the low activity region, ascending phase, high activity region, and descending phase respectively. (b) Distance, D for solar wind velocity corresponding to a) data.

range. During the ascending phase of the activity cycle (time series 9-12), D increases and reaches a maximum. In the high activity region (time series 13-17) D remains almost constant. During the descending phase of the activity cycle, *i.e.*, time series 17 to 18, D increases sharply.

5. Conclusions

Internal properties, structure, and dynamics of the solar wind vary spatially and temporarily (Balogh, Suess, and Lanzerotti, 2008). Solar wind is primarily divided into two components, a slow wind with velocities and a fast wind with velocities (Schwenn, 2007). Fast solar wind originates from relatively dark and cool regions in the corona, known as coronal holes (Feldman *et al.*, 1976). Solar wind originates from above the more active regions on the Sun. It is more

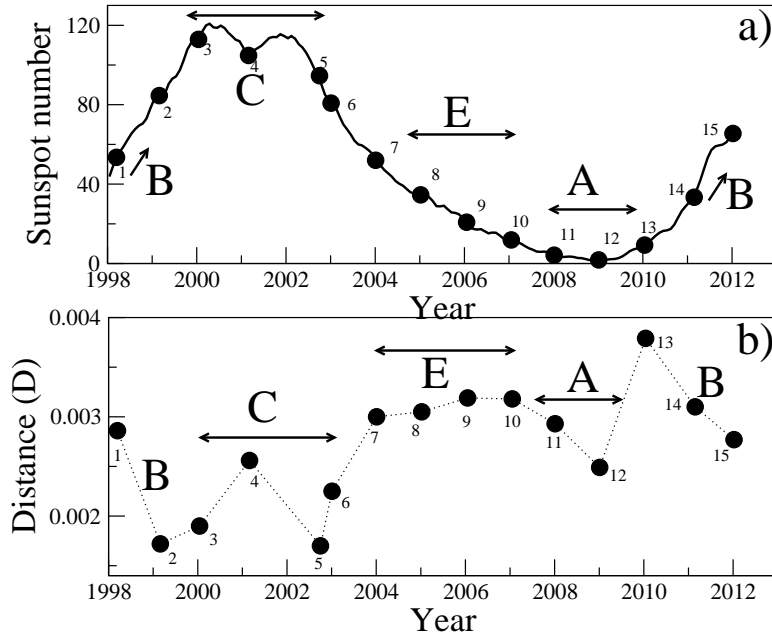


Figure 7. (a) Smoothed monthly averaged sunspot number from 1996 to 2012. Serial numbers 1 – 15 correspond to the solar wind data sets given in Table 2. Arrows with symbols A, B, C, and E indicate the low activity region, ascending phase, high activity region, and descending phase respectively. (b) Distance, D for solar wind velocity corresponding to a) data.

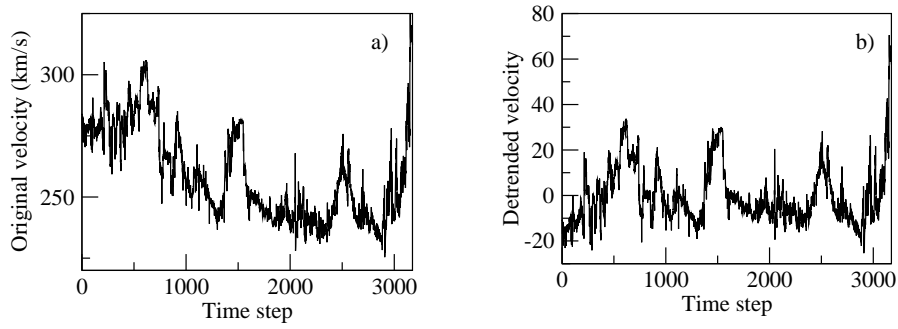


Figure 8. (a) Time series of solar wind velocity data obtained from Helios spacecraft correspond to data set of S. No. 16 of Table 3. (b) Detrended time series of a).

Table 3. Initial time (T), number of data points (N) of the 18 time series solar wind velocity data measured by the Helios 2 spacecraft from 1976 to 1982. Third column gives time irreversibility parameter, D (Eqn. 3). The last column gives daily averaged sunspot numbers (SSN).

S.No.	T	N	D	SSN
1	1975.181	3515	0.0064	20
2	1975.203	2938	0.0123	22
3	1975.704	2979	0.0078	17
4	1975.73	3083	0.0115	0
5	1976.205	2245	0.0068	38
6	1976.287	1843	0.0078	23
7	1976.791	1188	0.0116	13
8	1977.205	2741	0.0097	0
9	1977.287	3376	0.0042	31
10	1977.791	1085	0.0144	30
11	1978.286	2393	0.0155	116
12	1978.371	1911	0.0239	85
13	1979.370	1894	0.0043	158
14	1980.372	2218	0.0094	229
15	1980.454	2559	0.0078	152
16	1981.456	3174	0.0048	46
17	1981.458	2562	0.0064	109
18	1982.453	1361	0.0342	112

variable as compared to fast solar wind (Krieger, Timothy, and Roelof, 1973; Woo and Martin, 1997).

Time series irreversibility gives the information about the entropy production of the physical mechanism generating the time series (Roldán and Parrondo, 2010). In this paper, we present an analysis of solar wind velocity data obtained from two spacecrafts, ACE and Helios at distances 1AU and 0.3 AU respectively. We obtained several different time series of solar wind velocity from these two spacecrafts. These time series belong to different phases of solar activity cycles. To quantify the time irreversibility of these time series, we use DHVg algorithm and estimate the irreversibility parameter, D . A smaller value of D indicates a lesser time irreversible time series. Larger value of D indicates that the system generating the time series is a dissipative system.

We observe that D increases in the ascending phase of an activity cycle. After reaching to the maximum value, it decreases sharply in the high activity region of the activity cycle. Further, in the descending phase, D increases sharply, saturates in the low activity region and repeats the similar trend on the onset of new solar activity cycle. This shows that solar wind velocity is more variable during the high and low activity time, while less variable during the ascending and descending phases of the solar activity cycle. Variation of D over a solar activity cycle shows similar behavior for both the distances, *i.e.*, at 0.3 AU and 1 AU.

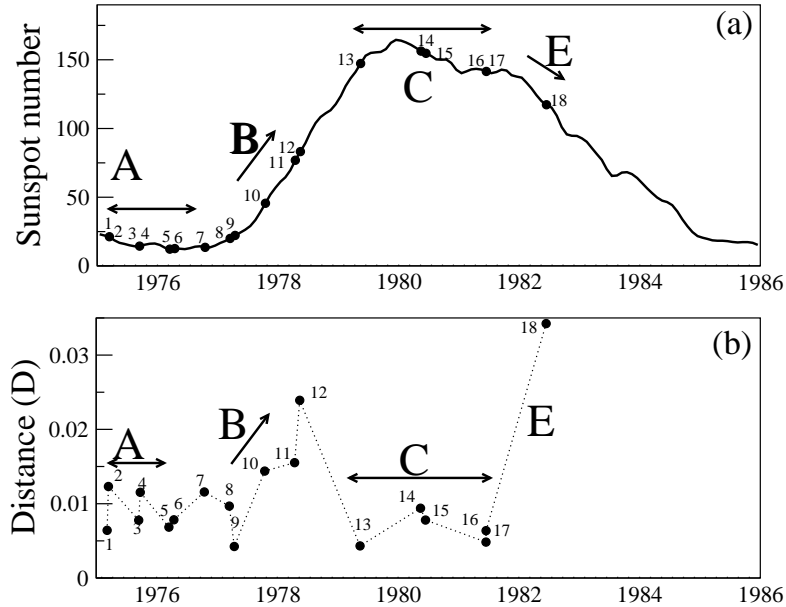


Figure 9. (a) Smoothed monthly averaged sunspot number from 1976 to 1985. Serial numbers 1–18 correspond to the Helios solar wind data sets given in Table 3. Arrows with symbols A, B, C, and E indicate the low activity region, ascending phase, high activity region, and descending phase respectively. (b) D from DHVg analysis for solar wind velocity corresponding to 9 (a) data.

Acknowledgements The authors thank the ACE Science Center and instrument teams for making available the ACE data used here. They thank Prof. Eckart Marsch, Max Planck Institute for Solar System Research, Lindau, Germany, for help in obtaining the Helios data. VS and AP thank CSIR for SRF, and Delhi University and DST Govt. of India for financial supports respectively.

References

- Arnold, V., Avez, A.: 1968, *Ergodic problems in classical mechanics*, Benjamin, NY.
- Balogh, A., Suess, S.T., Lanzerotti, L.: 2008, *The heliosphere through the solar activity cycle*, Praxis Publishing Ltd, Chichester, UK.
- Cover, T.M., Thomas, J.A.: 2006, *Elements of information theory*, Wiley, New Jersey.
- Feldman, W.C., Asbridge, J.R., Bame, S.J., Gosling, J.T.: 1976, *J. Geophys. Res.* **81**, 5054.
- Goldreich, P., Sridhar, S.: 1995, *Astrophys. J.* **438**, 763.
- Goldstein, M.L., Roberts, D.A., Matthaeus, W.H.: 1995, *Ann. Rev. Astron. Astrophys.* **33**, 283.
- Gupta, K., Prasad, A., Saikia, I., Singh, H.P.: 2008, *Planetary and Space Science* **56**, 550.
- Hansteen, V.H., Velli, M.: 2012, *Space Sci. Rev.* **172**, 89.
- Hapgood, M.A., Lockwood, M., Bowe, G.A., Wills, D.M., Tuluay, Y.K.: 1991, *Planetary and Space Science* **39**, 411.

- Katsavrias, C., Preka-Papadema, P., Moussas, X.: 2012, *Solar Phys.* **280**, 623.
- Krieger, A.S., Timothy, A.F., Roelof, E.C.: 1973, *Solar Physics* **29**, 505.
- Lacasa, L., Nuñez, A., Roldán, É., Parrondo, J.M.R., Luque, B.: 2012, *European Physical Journal B* **85**, 217.
- Macek, W.M., Obojska, L.: 1997, *Chaos Solitons and Fractals* **8**, 1601.
- Macek, W.M., Obojska, L.: 1998, *Chaos Solitons and Fractals* **9**, 221.
- Macek, W.M., Redaelli, S.: 2000, *Phys. Rev. E* **62**, 6496.
- McComas, D.J., Elliott, H.A., Schwadron, N.A., Gosling, J.T., Skoug, R.M., Goldstein, B.E.: 2003, *Geophysical Research Letters* **30**, 24.
- Milano, L.J., Dasso, S., Matthaeus, W.H., Smith, C.W.: 2004, *Phys. Rev. Lett.* **93**, 155005.
- Newman, M.E.J.: 2003, *SIAM Review* **45**, 167.
- Redaelli, S., Macek, W.M.: 2001, *Planet Space Sci.* **49**, 1211.
- Robinson, D.C., Rusbridge, M.G.: 1971, *Physics of Fluids* **14**, 2499.
- Roldán, É., Parrondo, J.M.R.: 2010, *Physical Review Letters* **105**, 150607.
- Rotter, T., Veronig, A.M., Temmer, M., Vršnak, B.: 2012, *Solar Phys.* **281**, 793.
- Schwenn, R.: 2007, *Solar dynamics and its effects on the heliosphere and earth, Space Sciences Series of ISSI*, Springer New York, 51.
- Shebalin, J.V., Matthaeus, W.H., Montgomery, D.: 1983, *Journal of Plasma Physics* **29**, 525.
- Stone, E.C., Frandsen, A.M., Mewaldt, R.A., Christian, E.R., Margolies, D., Ormes, J.F., Snow, F.: 1998, *Space Science Reviews* **86**, 1.
- Suyal, V., Prasad, A., Singh, H.P.: 2012a, *Solar Phys.* **276**, 407.
- Suyal, V., Prasad, A., Singh, H.P.: 2012b, *Planet Space Sci.* **62**, 55.
- Woo, R., Martin, J.M.: 1997, *Geophys. Res. Lett.* **20**, 2535.